Evaluation of the fretting fatigue behaviour of commercially pure titanium

C A R P Baptista[1*], **L S Rossino**[1], **M A S Torres**[2], and **C Y Shigue**[1]
[1]Department of Materials Engineering, EEL/USP, Lorena/SP, Brazil
[2] Department of Mechanics, FEG/UNESP, Guaratinguetá/SP, Brazil

The manuscript was received on 16 August 2006 and was accepted after revision for publication on 31 January 2007.

DOI: 10.1243/14644207JMDA122

Abstract: Fretting fatigue occurs when the contact surfaces of two components undergo small oscillatory movement while they are subjected to a clamping force. A cyclic external load gives rise to the early initiation of fatigue cracks, thus reducing their service life. In this paper, the fretting fatigue behaviour of commercially pure titanium flat samples (1.5 mm thick) is evaluated. A fretting device composed of a frame, load cell, and two screw-mounted cylindrical fretting pads with convex extremities was built and set to a servo-hydraulic testing machine. The fatigue tests were conducted under load control at a frequency of 10 Hz and stress ratio $R = 0.1$, with various contact load values applied to the fretting pads. Additional tests under inert environment allowed assessing the role of oxidation on the wear debris formation. The fracture surfaces and fretting scars were analysed via scanning electron microscopy in order to evaluate the surface damage evolution and its effect on the fatigue crack features. The effect of the fretting condition on the *S–N* curve of the material in the range of 10^4–10^6 cycles is described. Fatigue crack growth calculations allowed estimating the crack initiation and propagation lives under fretting conditions. The effect of the fretting condition in fatigue life is stronger for the lower values of cyclic stress and does not seem to depend on the contact loading value.

Keywords: fretting fatigue, titanium, fatigue life, surface damage

1 INTRODUCTION

The process known as fretting fatigue occurs at the contact surfaces of two components pressed together by a static load and is related to the simultaneous occurrence of wear, corrosion and fatigue damage. Small (usually less than 50 μm), relative cyclic slip at the interface between the two surfaces in contact induces friction stresses, wear, and surface damage. A cyclic external load applied to one or both the components gives rise to the early initiation of fatigue cracks [**1, 2**]. Fretting fatigue also leads to surface pitting and the transfer of metal from one surface to another. In addition, the small fragments of metal that are broken off oxidize, forming oxide particles, which, for most engineering metals, are harder than the metal itself. These become trapped between the mating surfaces and cause abrasive wear and scaring. As a consequence, a loss of fit between the two mating parts can occur [**3, 4**]. Fretting fatigue-related phenomena are present in several engineering applications, in which the bolted and riveted lap joints and dovetail connections are prominent examples [**5, 6**]. Unexpected failures under fretting fatigue conditions have been observed in many structural components at stress levels well below the fatigue limit of the material, which means that fretting can significantly reduce the fatigue strength of materials and structures [**7**]. A recent investigation on the propagation of fretting fatigue-nucleated cracks in Ti–6Al–4V showed that the fretting fatigue cycles had no effect on the residual strength of the material unless a crack of measurable depth (>50 μm) was nucleated by the fretting condition [**8**]. The specific failure mechanisms are influenced by factors such

Corresponding author: Department of Materials Engineering, Escola de Engenharia de Lorena, Polo Urbo industrial, Gleba Al-6, Cx. Postal 116, CEP 12602-810, Lorena SP, Brazil. email: baptista@demar.eel.usp.br

as the geometry and properties of the contacting bodies, the lubricant, if any, between the surfaces, the topology of the surfaces, loading conditions, and environment. These mechanisms may include phenomena such as delamination, which is a result of adhesive wear combined with ductility exhaustion and leads to microcrack initiation beneath the surface, and friction leading to crack initiation and growth due to cyclic tangential stresses promoted by combining frictional force along the contact surface and bulk alternating stress [**1**]. To investigate the characteristics of fretting fatigue, various test apparatus have been developed and described in the literature. They can differ, for example, with regard to the test sample, pad geometry (flat, spherical, cylindrical, bridge-type), and normal load transmission (hydraulic actuator, loading ring, spring, and so on) [**2**, **4–6**, **9**, **10**].

Because of its very favourable properties, which include high strength-to-weight ratio and corrosion resistance, titanium is one of the most important structural materials, suitable for a wide range of applications [**11**]. The replacement of other materials with titanium in various applications, such as chemical processing equipments, aircraft parts, and medical implants, leads to a growing interest in the fatigue characteristics of this material. Titanium and its alloys are known for showing a high ratio of fatigue resistance to ultimate strength [**12, 13**]. Early studies of fatigue properties of various grades of commercially pure titanium showed the presence of a fatigue limit in their stress life (S–N) curves, which was attributed to the difficulty in developing fatigue striations in a sufficiently large number of grains [**14**]. It was also observed that imperfections such as large rolled-in surface defects have no influence on room-temperature fatigue performance of ASTM grade 2 strip specimens [**15**]. However, fretting fatigue data on this material are scarce. Recently, the conspicuous effect of fretting on the fatigue strength of medical-grade titanium alloys Ti–6Al–4V and Ti–6Al–7Nb was demonstrated, and some surface coatings were tested aiming to reduce damage severity [**16**]. In that work, the fretting fatigue failures of titanium alloys were characterized by the formation of oxides due to the generation of high temperature from friction. In the present work, commercially pure (ASTM grade 2) annealed titanium flat samples are subjected to fretting fatigue experiments using convex-ended pads and a displacement-controlled apparatus in which an initial contact load is set and let evolve as the axial cyclic loading is applied to the specimens. The objectives of the work include the assessment of the contact load evolution and the effect of the fretting condition on the S–N curve of the material. Calculations of the crack growth cycles allowed estimating the initiation and propagation lives under fretting conditions. Moreover, the fretting scars were analysed via scanning electron microscopy, in order to evaluate the surface damage evolution.

2 EXPERIMENTAL DETAILS

Commercially pure (ASTM grade 2) titanium flat samples, cut from an annealed sheet (1.5 mm thick), were tested in this work. From microstructural analysis, it was possible to confirm that this material presents equiaxed grains with an average grain diameter of 28 μm. The basic mechanical properties, obtained from tensile tests, are the following: yield strength = 349 MPa, ultimate tensile strength = 488 MPa, Young's modulus = 103 GPa and elongation to fracture = 27 per cent. The fatigue crack propagation properties for load ratio $R = 0.1$ were obtained in a previous work [**17**] in terms of the Paris law parameters and are given in equation (1), in which $\mathrm{d}a/\mathrm{d}N$ is the fatigue crack growth rate (m/cycle), and ΔK is the stress intensity factor range (MPa m$^{1/2}$). For the present work, a specimen configuration with continuous radius between ends, whose dimensions followed the recommendations of ASTM E466 standard, was adopted. The test pieces were carefully ground with emery paper from #400 to #800.

$$\frac{\mathrm{d}a}{\mathrm{d}N} = 8.14 \times 10^{-11}(\Delta K)^{2.84} \tag{1}$$

A fretting device composed of a frame, load cell, and loading screws, as shown in detail in Fig. 1, was built and set to a servo-hydraulic testing machine. The load cell was connected to a data-acquisition system operating at a sampling rate of 50 Hz. Convex-ended (radius = 20 mm) cylindrical titanium fretting pads were fitted to the extremities of the loading screws. Transverse reinforcements were also fitted to the fretting device in order to minimize the bending deflection of the pad supports.

The conventional and fretting fatigue tests were performed at room temperature in laboratory air under load control. The tests were run with a stationary sinusoidal cyclic loading (frequency = 10 Hz) and $R = 0.1$. The maximum stress levels of the load cycle were chosen in such a way that the achieved fatigue lives lied in the range of 10^4–10^6 cycles. The experimental program included various nominal contact load values for the fretting fatigue tests ($P = 100$, 300, 500, and 900 N), as well as some additional tests under inert (argon) atmosphere. Some of the tests were interrupted before final fracture in order to allow observing the fretting process evolution. The post-mortem microscopic analyses were performed using a LEO 1450VP SEM in the secondary electrons mode.

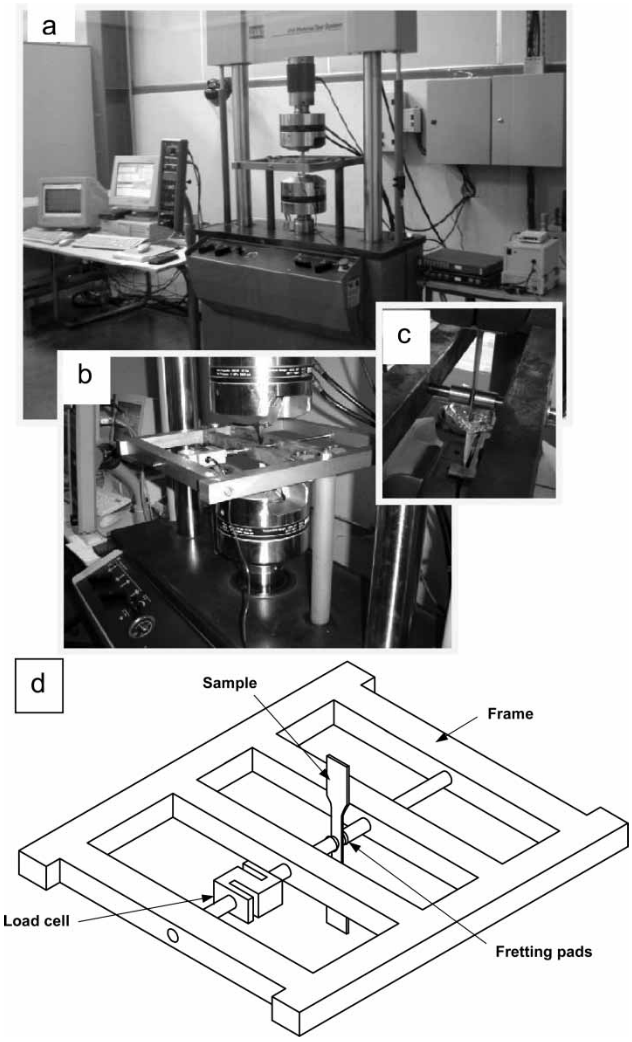

Fig. 1 Experimental apparatus: (a) general view of testing machine and data acquisition system; (b) fretting fatigue experimental setup; (c) detail of test piece clamped to fretting pads; (d) schematic of test setup

3 RESULTS AND DISCUSSION

Three main aspects of the results obtained are discussed: contact load variation during the tests, fretting fatigue damage evolution, and fatigue life data.

3.1 Contact load variation

Fretting fatigue experiments usually use a hydraulic actuator in order to keep constant the contact load. However, this practice does not reproduce the fretting condition of some real components, such as bolted joints or riveted parts. In the present work, after the initial setting of the contact load value, its variation was recorded as the fatigue test proceeded. The collected data allowed verifying that the contact load P has a small oscillating component, which can be related to the cyclic loading applied to the specimen, and an average component that reflects the evolution of P. A good description of the latter was achieved through polynomial fit of order 9 and the results are shown graphically in Fig. 2(a) for some experimental conditions. By plotting the average P-value against the number of cycles, a similar behaviour consisting of an initial huge drop followed by a tendency to asymptotic behaviour was observed for all loading conditions. The initial drop is related to surface accommodation, and the asymptotic behaviour is probably due to the wear and damage evolution. The initial drop duration was found to vary between 1×10^3 and 5×10^3 cycles and, although its height increases as P is increased, its normalized values

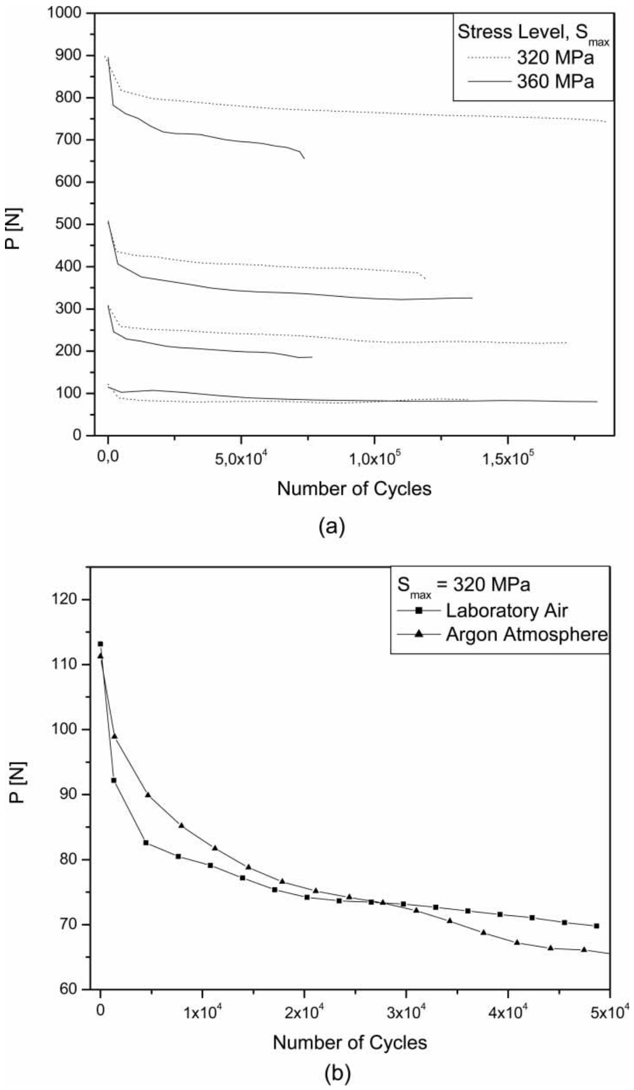

Fig. 2 Graphical representation of mean contact load evolution during fatigue tests: (a) various loading conditions in laboratory air; (b) comparison of tests run in laboratory air and argon atmosphere

decrease from about 30 per cent for $P = 100\,\mathrm{N}$ to 10 per cent for $P = 900\,\mathrm{N}$. In general, for a given contact load, its variation increases with the increase in the maximum cyclic stress value, $S_{\max}$. This behaviour is associated with the accumulated sliding distance of the fretting pads over the test piece surface: the higher $S_{\max}$, the higher the test piece deformation and of course the sliding width for each loading cycle. Despite these observed tendencies, some fluctuation can occur in the average P-values, possibly related to third-body formation during the wear process. As for the argon atmosphere tests, no significant change was observed in the contact load behaviour (Fig. 2(b)), although the generated wear particles were quite different.

3.2 Surface damage

It was observed that, during the early stages of the fretting process, the surface region corresponding to the contact area becomes rougher. It is believed that the main mechanism acting in this stage is the adhesive wear. Figure 3 shows the specific feature, called fretting scar, which develops in the surface of the sample (Fig. 3(a)) and gives rise to nucleation and growth of micro cracks (Fig. 3(b)). As the test proceeds, the fretting scar acquires a slightly elongated shape because of the creep deformation suffered by the specimen during the asymmetric fatigue cycles. It must be reminded that the crosshead, together with the fretting device, remains fixed during the tests, whereas the actuator moves up and down when applying the cyclic loading. If creep deformation occurs, the displacement range of the actuator changes in order to keep the steady-state loading regime, thus moving the contact point towards the upper side of the specimen. Because the contact point is not fixed, crack nucleation can occur at different sites within the contact region. Furthermore, the magnitude of relative slip between the surfaces in contact has not a prescribed value, being dependent on other variables such as the adopted cyclic load, contact load, and compliance of the fretting device. Estimates based on the specimen

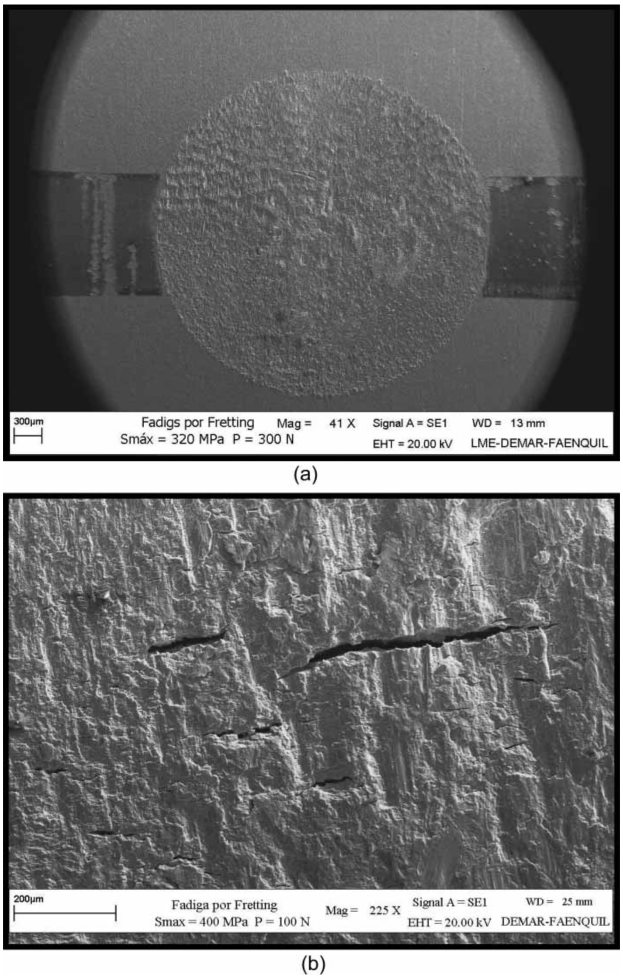

Fig. 3 Fretting scar: (a) general view; (b) microcracks

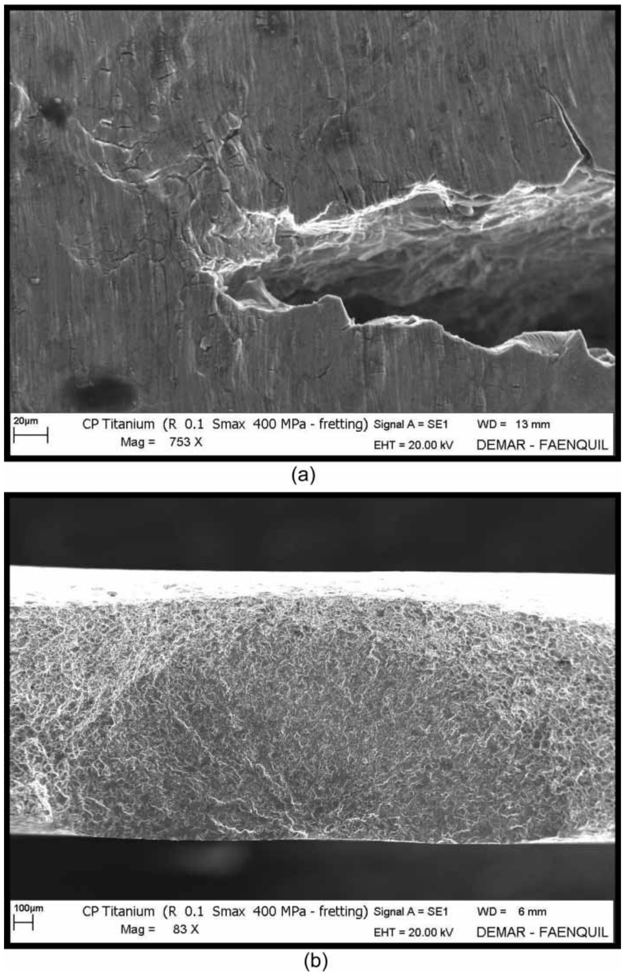

Fig. 4 Fretting fatigue features: (a) border of a growing crack at the specimen surface; (b) typical fracture appearance

deformation resulted in slip ranges from 50 to 120 μm for the fretting conditions adopted in this work.

Figure 4 shows the formation of a main crack (Fig. 4(a)) as a result of micro crack coalescence and the fracture surface (Fig. 4(b)) created by its growth. Delamination evidences at the contact area can be seen near the border of the propagating crack shown in Fig. 4(a). The delamination process causes the metal fragments to dig up, leading to debris formation and giving rise to abrasive wear. The fracture surfaces of the tested samples presented distinct crack initiation sites for the conventional and fretting fatigue tests: in the former case, cracks nucleated at the corners of the test pieces, and in the latter case, cracks nucleated at the contact area between the sample and the fretting pad. The most common situation for the fretting fatigue tests referred to crack propagation from one of the faces, thus resulting in fracture surfaces in which the fatigue cracks had semi-elliptical shape, as shown in Fig. 4(b).

Some additional tests were performed under inert environment (argon atmosphere). In this case, the test piece clamped to the fretting pads was evolved by an elastic rubber chamber into which a positive pressure was kept constant by means of an injected steady argon flow. Figure 5 shows a comparison of wear particles generated in tests carried out under laboratory air (Fig. 5(a)) and argon atmosphere (Fig. 5(b)). In the first case, it can be seen that the particles were successively broken into smaller pieces, which evidences their brittle nature. Although some of the wear particles remained trapped in the fretting scars, a considerable amount of material was thrown outside this region in the form of dark debris. Microanalyses via energy dispersion spectrometry (EDS) detected the presence of titanium oxides in these sites. Although it was not possible to precise the oxide stoichiometry, this discovery confirms the role of oxygen as wear particle embrittlement agent. On the other hand, the needle-shaped particles that can be seen in Fig. 5(b), probably formed by rolling between the specimen and pad surfaces, were found only in tests ran under argon atmosphere. Of course, the deformation process by which the particles acquired this shape was allowed to occur because the particles remained ductile in the inert environment. No systematic investigation was made in the present work on how the environment affects the fatigue life, but the fretting scars appearance suggests that the rolling of the ductile particles tends to lessen abrasive wear. Further research is to be done.

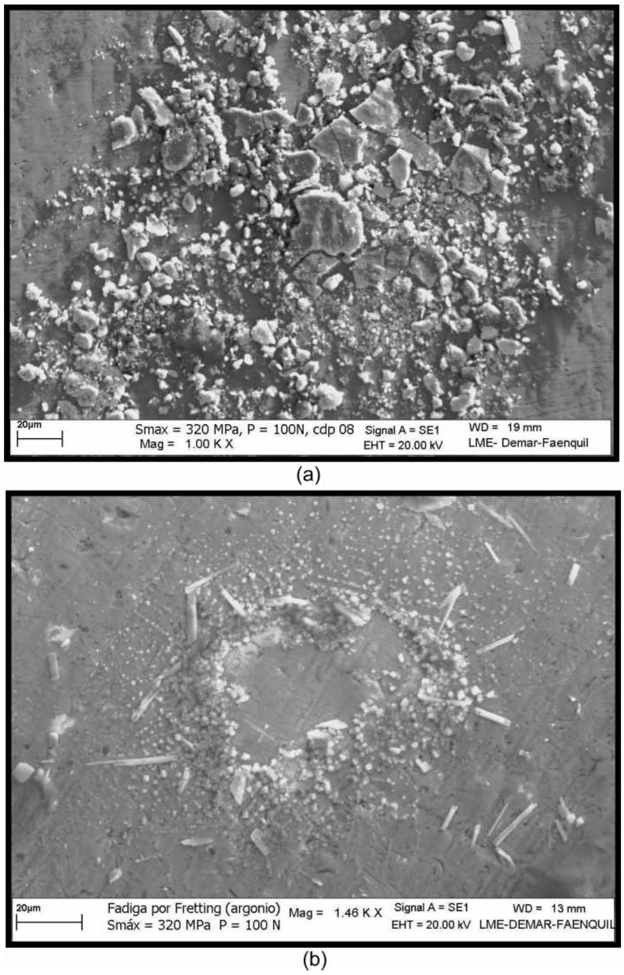

Fig. 5 Wear particles formed: (a) in laboratory air; (b) in argon atmosphere

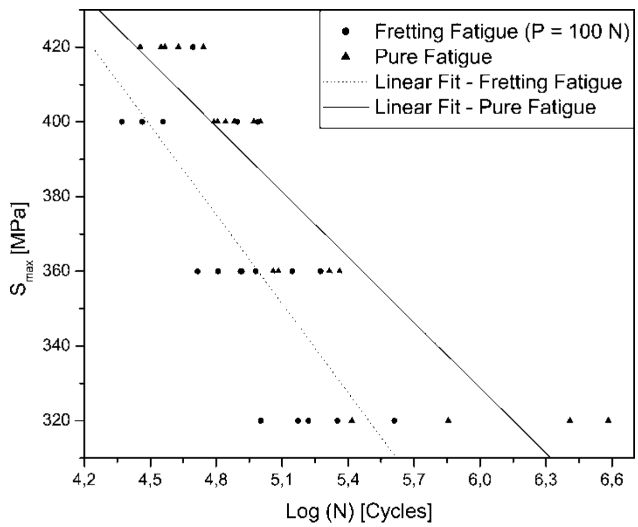

Fig. 6 Pure and fretting fatigue life curves

3.3 Fretting fatigue life

The results of pure and fretting fatigue tests performed with a nominal P-value of 100 N are plotted in Fig. 6. The fatigue curves were obtained by linear fitting through the least squares method. It can be seen that the effect of the fretting condition on the average fatigue life increases as the maximum nominal cycle stress decreases. For example, the calculated life reduction is 50 per cent at 400 MPa and 80 per cent at 320 MPa. This is in part explained by the fact that the fretting process basically affects crack initiation, and this portion of fatigue life is expected to present a relative increase for lower stress amplitudes. Thus, the fatigue life reduction due to fretting should be basically a decrease in the crack initiation cycle number when compared with the pure fatigue condition. Furthermore, the analysis of the fractured specimens allowed observing that, at the stress level $S_{max} = 420$ MPa, simultaneous fatigue and fretting fatigue crack initiation were possible. In this case, the total fatigue life observed in fretting experiments was the same as for the conventional fatigue. These tests were not considered 'fretting fatigue' results.

The two-parameter Weibull distribution was employed to describe the fatigue life behaviour of the material. The cumulative distribution function is given by equation (2), in which $F(N)$ is the probability of failure at a number of cycles up to N, α is the characteristic life (the scale parameter), being the number of cycles corresponding to the failure probability of 63.2 percent, and β is the slope (or shape parameter) representing the data scattering. At least five test data were employed in the Weibull parameters calculation for each condition. The results are shown in Table 1 ($P = 0$ indicates pure fatigue tests). From the calculated β-values, a general tendency is observed for the scattering in fatigue life: the scattering decreases with the increase in S_{max} and P-values (bigger β-values indicate less data scattering). Table 1 also confirms statistically, for all the fretting conditions, the observations made from Fig. 6 for $P = 100$ N: the α-values show that the effect of fretting is increased as the cyclic stress decreases. Moreover, it can be seen that the α-values for all of the contact loads at 320 and 360 MPa are of the same magnitude, making it evident that the contact load does not significantly affect the fretting fatigue life

$$F(N) = 1 - \exp\left[-\left(\frac{N}{\alpha}\right)^{\beta}\right] \quad (2)$$

Measurements of the fracture surface area dimensions corresponding to the stable crack growth regime were done for the test pieces fretted at $P = 100$ N. These semi-elliptical cracks presented a/c (depth to half-width) ratios varying from 0.65 to 0.89. The average final crack depth value a_f was determined from the experimental observations and is given in Table 2. Fatigue striations were found in the stable crack growth region of all the specimens. Striation spacing (ss) measurements were performed at the mid-thickness of the samples. At least three measures were taken in each specimen; then the average values of ss were calculated for each stress level and is given in Table 2. It was shown in a previous work [**17**] that a one-to-one relationship between macroscopic crack growth rate and striation spacing is valid for ASTM grade 2 titanium when ss $\geqslant 0.3\,\mu$m. If an expression for the stress intensity factor of these cracks is available, it can be employed together with equation (1) in order to estimate the theoretical crack growth rate at mid-thickness, whose values could be compared with the striation spacing measurements. It should be noted that, for high strain-hardening materials (such as the commercially pure titanium used in this work), the use of equation (1) – based on linear elastic fracture mechanics – could be extended beyond the elastic limit, allowing mean plastic deflections to occur in the specimen. However, these mean deflections can accelerate growth rates by as much as a factor of two [**18**].

The mode I stress intensity factor range at a semi-elliptical crack in a finite width plate is given by equation (3), in which R is the stress ratio, S_{max} the maximum nominal cyclic stress, a the crack depth, and Q the shape factor for an ellipse, given by the square of the complete elliptic integral of the second kind. The boundary correction factor $Y(a/t, a/c, \phi)$ is a function of crack depth, crack length, plate thickness, and the parametric angle of the ellipse. Raju and Newman [**19**] calculated values of Y for various semi-elliptical surface cracks in finite-thickness plates. Taking these values and performing some interpolations, we were able to estimate the ΔK values corresponding to the fretting-generated cracks, and using equation (1), we obtained the estimations

Table 1 Weibull parameters of fatigue life for pure ($P = 0$) and fretting fatigue

	$S_{max} = 320$ MPa		$S_{max} = 360$ MPa		$S_{max} = 400$ MPa	
P (N)	β	α	β	α	β	α
0	0.6801	2 244 903	2.3284	209 736	4.9264	84 137
100	1.5877	239 273	2.0444	116 463	1.3325	63 899
300	1.3229	305 699	2.1943	115 010	–	–
500	3.2246	141 411	3.7512	131 709	–	–
900	6.0487	192 236	3.2853	121 862	–	–

Table 2 Striation spacing and crack growth rate at mid-thickness for fretting fatigue samples

S_{max} [MPa]	a_f (mm)	ss (μm)	da/dN (μm/cycle)
320	1.44	0.36	0.44
360	1.35	0.64	0.60
400	1.23	0.73	0.83

Table 3 Fatigue life and crack propagation cycles (N is the average of five results)

S_{max} [MPa]	N (cycles)	N_p (cycles)	N_p/N (%)	N_i/N (%)
320	338 844	17 587	5.2	94.8
360	100 940	12 464	12.3	87.7
400	31 620	9136	28.9	71.1

of da/dN at mid-thickness given in Table 2. It can be obtained that these values correlate well to the average ss for each experimental condition. This fact encourages estimating the residual life of the cracked specimens, even if some conservatism is expected to occur in the computations. Considering that the total fatigue life is divided into initiation (N_i) and propagation (N_p) cycles, simple numerical integrations of equation (1) were performed in order to estimate the life portion consumed in the crack propagation stage. In these calculations, it was assumed an initial crack depth $a_0 = 0.1$ mm (circa three grain sizes) and also that the a/c ratio (measured at the fracture surface) remained constant as the crack grew. The results obtained are shown in Table 3 together with the average total fatigue life for each condition. Hence, the percentages of fatigue life spent in crack initiation and crack propagation were also estimated and placed in the last two columns of Table 3. These results show the relative decreasing of crack initiation cycles as the cyclic stress is increased

$$\Delta K = (1 - R) \cdot Y\left(\frac{a}{t}, \frac{a}{c}, \phi\right) \cdot S_{max} \cdot \sqrt{\left(\pi \cdot \frac{a}{Q}\right)} \quad (3)$$

4 CONCLUSIONS

From the results presented in this work, referred to fatigue in ASTM grade 2 titanium sheet samples fretted against screw-mounted convex titanium pads, the following conclusions can be drawn.

1. The contact load suffers an initial drop (10–30 per cent) and evolves asymptotically during the cyclic loading. Because of the higher accumulated sliding distance of the fretting pads over the contact surface, the variation in contact load increases with the increase in the cyclic stress.
2. Flat samples present semi-elliptical cracks when subjected to fretting. The shape of the wear particles as well as the surface roughness is affected by the environment. The absence of oxidation (which causes metal embrittlement) allows the detached fragments to acquire a needle-like format by rolling between the contacting surfaces.
3. The effect of fretting condition in fatigue life is stronger for the lower values of cyclic stress and does not seem to depend on the contact load value.

REFERENCES

1 **Mutoh, Y.** Mechanisms of fretting fatigue. *JSME Int. J.*, 1995, **38**, 405–415.

2 **Jin, O.** and **Mall, S.** Influence of contact configuration on fretting fatigue behaviour of Ti–6Al–4V under independent pad displacement conditions. *Int. J. Fatigue*, 2002, **24**, 1243–1253.

3 **Frost, N. E., Marsh, K. J.,** and **Pook, L. P.** *Metal fatigue*, 1999, pp. 364–370 (Dover Publications, New York).

4 **Elliot, C. B.** and **Hoeppner, D. W.** The importance of wear and corrosion on the fretting fatigue behavior of two aluminium alloys. *Wear*, 1999, **236**, 128–133.

5 **Hutson, A., Nicholas, T.,** and **Goodman, R.** Fretting fatigue of Ti–6Al–4V under flat-on-flat contact. *Int. J. Fatigue*, 1999, **21**, 663–669.

6 **Birch, P. R.** *A study of fretting fatigue in aircraft components.* Master Thesis, Massachussetts Institute of Technology, Cambridge, 1998, p. 152.

7 **Hattori, T.** Fretting fatigue problems in structural design. *ESIS 18: Fretting fatigue*, 1994, pp. 437–451 (Mechanical Engineering Publications, London).

8 **Hutson, A., Nicholas, T.,** and **John, R.** Fretting fatigue analysis in Ti–6Al–4V. *Int. J. Fatigue*, 2005, **27**, 1582–1589.

9 **Venkatesh, T. A., Conner, B. P., Lee, A. E., Giannakopoulos, A. E., Lindley, T. C.,** and **Suresh, S.** An experimental investigation of fretting fatigue in Ti–6Al–4V: the role of contact conditions and microstructure. *Metall. Mater. Trans. A*, 2001, **32A**, 1131–1146.

10 **Lindley, T. C.** and **Nix, K. J.** An appraisal of the factors which influence the initiation of cracking by fretting in power plant. *ESIS 18: Fretting fatigue*, 1994, pp. 239–256 (Mechanical Engineering Publications, London).

11 **Donachie, M. J.** *Titanium: a technical guide*, 1988, p. 469 (ASM International, Metals Park).

12 **Rhode, T. M.** and **Ertel, P. W.** Constant amplitude fatigue life data for notched and unnotched annealed Ti–6Al–4V sheet. Technical Report AD A193 420/7/XAB, Wright–Patterson Air Force Base, Ohio, 1988, p. 38.

13 **Baptista, C. A. R. P., Schneider, S. G., Taddei, E. B.,** and **Silva, H. M.** Fatigue behavior of arc melted Ti–13Nb–13Zr alloy. *Int. J. Fatigue*, 2004, **26**, 967–973.

14 **Turner, N. G.** and **Roberts, W. T.** Fatigue behavior of titanium. *Trans. Metall. Soc. AIME*, 1968, **242**, 1223–1230.

15 **Wardlaw, T. L.** and **Hall, J. A.** Fatigue properties of commercially pure titanium. In *Industrial applications of titanium and zirconium* (Ed. E. W. Kleefisch), 1981, pp. 45–58, ASTM STP728 (ASTM, Philadelphia, USA).

16 **Vadiraj, A.** and **Kamaraj, M.** Damage characterization of unmodified and surface modified medical grade titanium alloys under fretting fatigue condition. *Mater. Sci. Eng. A*, 2006, **416**, 253–260.

17 **Rossino, L. S., Baptista, C. A. R. P.,** and **Rodrigues, D., Jr.** Microscopic features related to fatigue crack growth in commercial-purity titanium. In Proceedings of the 8th

International Fatigue Congress (Ed. A. F. Blom), 2002, pp. 1797–1804 (EMAS: Cradley Heath).
18 ASTM E 647-95a. Standard test method for measurement of fatigue crack growth rates. *Annual book of ASTM standards*, vol. 03.01, 1997, pp. 557–593 (ASTM, West Conshohocken, USA).
19 **Raju, I. S.** and **Newman, J. C. Jr.** Stress-intensity factors for a wide range of semi-elliptical surface cracks in finite-thickness plates. *Eng. Fract. Mech.*, 1979, **11**, 817–829.

APPENDIX

Notation

a	crack length; depth of semi-elliptical crack
a_f	average final crack depth
a_0	initial crack depth
da/dN	fatigue crack growth rate
$F(N)$	probability of failure occur at a number of cycles up to N
N	number of cycles representing the total fatigue life
N_i	number of cycles for crack initiation
N_p	number of cycles for crack propagation
P	contact load
Q	shape factor of an ellipse
R	stress ratio (minimum to maximum) of a loading cycle
S_{max}	maximum nominal stress of a cyclic loading
ss	striation spacing
Y	geometry correction factor for ΔK
α, β	scale and shape parameters of Weibull probability function
ΔK	stress intensity factor range